Journal of Molecular Liquids 388 (2023) 122759

Contents lists available at ScienceDirect

Journal of Molecular Liquids

journal homepage: www.elsevier.com/locate/molliq

Towards green flotation: Investigating the effect of rhamnolipid biosurfactant on single bubble adhesion dynamics

Krzysztof Jan Legawiec [a,*], Mateusz Kruszelnicki [a,*], Michalina Zawadzka [b], Pavlína Basařová [c], Jan Zawala [d], Izabela Polowczyk [a]

[a] Department of Process Engineering and Technology of Polymer and Carbon Materials, Wroclaw University of Science and Technology, 27 Wybrzeże Wyspiańskiego St., 50-370 Wrocław, Poland
[b] Group of Peptide Engineering, Faculty of Chemistry, Wrocław University, 14 Joliot-Curie St., 50-383 Wrocław, Poland
[c] Department of Chemical Engineering, University of Chemistry and Technology, Prague, 5 Technická St., 166 28 Praha, Czech Republic
[d] Jerzy Haber Institute of Catalysis and Surface Chemistry Polish Academy of Sciences, 8 Niezapominajek St., 30-239 Kraków, Poland

ARTICLE INFO

Keywords:
Green flotation
Three-phase contact
Frother
Glycolipid biosurfactant
Rhamnolipids

ABSTRACT

In this study we performed an experimental analysis of the influence of rhamnolipid (RL) biosurfactant produced by *Pseudomonas aeruginosa* on the dynamics of bubble adhesion onto model surfaces of various hydrophobicity. The attachment time of a single bubble to a solid surface with contact angles of 6, 34, 49 and 80° was evaluated at different concentrations of RL in the range of 0 to 500 mg·dm^{-3}, both at pH 5 (non-ionic form) and pH 10 (anionic form). The dependence of the three-phase contact (TPC) formation time on biosurfactant concentration was determined by monitoring the bubble-solid surface interactions using a high-speed camera. It was found that as the concentration of RL rises, the formation time of the TPC extends as a result of an increase in the film drainage time. A significant effect of RL on the process of TPC expansion (lower rate) and the size of the contact area between the bubble and the surface (smaller surface area) was also noted. This study provides a better understanding of the effect of one of the most popular biosurfactants on the fundamental act of the flotation process: attachment of the particle to the bubble.

1. Introduction

Froth flotation is a separation technique that exploits the differences in the physical and surface properties of the mineral particles. The process involves the collision of gas bubbles and particles, where if the particle exhibits a sufficient level of hydrophobicity, attachment between these objects will occur. Attachment is essential to the flotation process, determining its overall effectiveness [1,2]. When a bubble and a particle collide, a thin film of liquid is formed between them, the stability of which determines whether three-phase contact (TPC) formation will occur [1]. This stability is determined by the different kinds of interactions between the surfaces of a solid and a bubble, such as electrostatic, van der Waals, and hydrophobic [3]. Analysis of the mechanism of attachment of the solid particle to the gas bubble is of great importance in understanding and improving the flotation process [4]. For example, it has already been proven that there is a correlation between the three-phase contact formation time and flotation efficiency [5]. The authors stated that the TPC formation time is one of the basic parameters that affect the successful attachment of particles to bubbles. It has also been shown that the shorter this time is, the higher is the flotation yield obtained. The research of Kowalczuk and co-workers demonstrates the crucial role of the thin liquid film stability and kinetics of three-phase contact formation by colliding bubbles with a solid surface.

Chemicals such as collectors, frothers, and modifiers are applied [6] to control process parameters and improve efficiency [6]. Collectors are used to selectively adsorb onto the surface of the target mineral grain and enhance its hydrophobicity. In contrast, frothers, which are surface-active agents, are used to improve gas dispersion by creating smaller bubbles and establishing a froth layer with a desirable level of stability. Currently, these are primarily compounds of synthetic (petrochemical-based) origin. The aspiration towards sustainability in the flotation process is associated with a number of efforts to introduce substitutes for synthetic substances into industrial operations. One idea to replace the petroleum-based molecules employed to control processes is the application of bioproducts [7,8]. In particular, this trend is noticeable for

* Corresponding authors.
E-mail addresses: krzysztof.legawiec@pwr.edu.pl (K.J. Legawiec), mateusz.kruszelnicki@pwr.edu.pl (M. Kruszelnicki).

https://doi.org/10.1016/j.molliq.2023.122759
Received 11 April 2023; Received in revised form 2 August 2023; Accepted 3 August 2023
Available online 4 August 2023

systems where it is necessary to modify the properties of the phase boundaries. Modification of these properties on an industrial scale, especially in separation processes, is achieved by adding surface-active compounds to the system [9]. Through adsorption at the interface, these molecules provide physicochemical changes in surface properties. However, conventionally used surfactant molecules can be poorly biodegradable and harmful to humans and aquatic organisms [10]. Therefore, one of the more important advances is the use of surfactants secreted extracellularly by bacteria – biosurfactants.

Mineral flotation has been greatly improved by the use of microbial products such as biosurfactants and organic acids. Extensive research has been conducted on rhamnolipid biosurfactants produced by strains of *Pseudomonas aeruginosa*. Two primary types of rhamnolipids (RL), mono- and di-RL, are typically produced during standard growth conditions, and both have two hydrophobic chains [11]. Due to its ability to complex divalent ions, RL has already been tested as a collector in precipitation flotation of cadmium(II) [12,13], chromium [14,15], uranium [16], lanthanum(III) and caesium (I) [17], and many other rare earth elements. The hydrogen bonding ability paved the way to use these biomolecules in other processes, such as removal of dyes [18–20] and even dewatering of oily sludges from dissolved air flotation processes in petroleum refineries [20,21], where RL showed the ability to break up the emulsified oil droplets. RL has also been studied as a potential frothing agent leading to increased grades and recoveries of molybdenum and copper in copper ore flotation [22], as well as in coal flotation [23,24]. The results showed that RL had greater surface activity and frothing ability than MIBC (methyl isobutyl carbinol) and DOW-250 (DOWFROTH 250) due to the significantly higher molecular weight and the presence of multiple oxygenated functional groups in its molecule. RL showed substantially better results than conventional synthetic reagents in many of these cases. Despite promising results, the optimal use of rhamnolipid in flotation is still an area of ongoing research. Factors such as optimal concentration and pH must be carefully considered to maximise the performance of RL in the flotation process. Additionally, the economic feasibility of using the concerned molecules on an industrial scale must be evaluated.

This paper presents the results of a study on the influence of pH and concentration of RL biosurfactant on the kinetics of three-phase contact formation on quartz plate surfaces with different hydrophobicity. Experiments were carried out in solutions containing a mixture of RL homologues with a di- to mono-RL ratio of 0.3. By changing the pH of the solution, the ability of RL molecules to act as non-ionic and anionic surfactants was demonstrated. The mechanism of TPC formation is broadly discussed to shed light on the insights gained by the study.

To date, this is the first paper to focus on the adhesion of the bubble to the solid, the fundamental act of flotation, in the presence of rhamnolipid, directly explaining its effect on the stability of the thin wetting film.

2. Materials and methods

2.1. Materials

Rhamnolipid biosurfactant (RL) was purchased from AGAE Technologies LLC (Corvallis, OR, USA) as a mixture of different mono- and di-RL homologues. Individual RL congeners present in the supplied mixture were identified by the LCMS-IT-TOF technique (ion trap/time-of-flight mass spectrometry coupled with high-performance liquid chromatography). A sample of RL was dissolved in a mixture of water and acetonitrile (50:50). The LC-MS experiment was performed on a Shimadzu IT-TOF instrument with an electrospray ion source in negative ion mode. Separation was carried out on an Aeris PEPTIDE 3.6 μm XB-C18 column (50 × 2.1 mm) with a gradient elution of 5–90% B in A (A = 0.1% HCOOH in water; B = 0.1% HCOOH in MeCN) at room temperature for 15 min (flow rate: 0.2 ml·min^{-1}).

The LC-MS chromatogram showed signals corresponding to 7 RL homologs: 2 di-RL and 5 mono-RL. The three mono-RL homologs can exist as isoforms (Rha-C_{10}-C_8/Rha-C_8-C_{10}, Rha-C_{10}-$C_{12:1}$/Rha-$C_{12:1}$-C_{10} and Rha-C_{10}-C_{12}/Rha-C_{12}-C_{10}; note that Rha is an abbreviation representing the hydrophilic portion of biosurfactant – the rhamnose molecule) and one of them consists of an unsaturated bond. The relative abundance of each component was calculated based on the area under the chromatogram signals. Mono-RL homologues predominated in the sample, and the most abundant homolog was Rha-C_{10}-C_{10}. The ratio of di-RL to mono-RL was 23.89:76.11 (~0.3), wherein Rha-C10-C10 constituted 39.63% of the total RLs. The data obtained are shown in Table S1. The average molar mass of the biosurfactant used was 499.60 g·mol^{-1}.

Fused quartz microscope slides were used as a model solid substrate for thin film stability measurements (Alfa Aesar, USA). The chemical composition of the slides was obtained by X-ray fluorescence spectroscopy (Epsilon 3X, PANalytical, USA). The main chemical component was SiO_2, constituting 99.5 ± 0.1%, and Al_2O_3, TiO_2, and CaO in the amounts of 0.2, 0.2, and 0.1%, respectively. Surface roughness of non-modified plate was analysed using an optical profilometer (Contour GT, Veeco). The roughness parameters were evaluated based on measurements taken at ten random locations, each with an area of 1.3 × 0.9 mm. Average roughness (R_a) was 3.9 ± 1.4 nm while root mean square roughness (R_{RMS}) was 5.0 ± 1.7 nm.

N-alkyl alcohols – 1-propanol (99%), 1-butanol (99%), and 1-octanol (99%) – were used for quartz plates' surface esterification and were purchased from Alfa Aesar (MA, USA). Methanol, acetone, sulphuric acid (95%), hydrochloric acid (35–38%) used in glass cleaning, hydrochloric acid (1 M) and sodium hydroxide (1 M) for pH adjustment and sodium chloride used as a background electrolyte were analytical grade and were purchased from Avantor Performance Materials Poland S.A. (Poland). Solutions were prepared using ultrapure water with a conductivity of 0.05 μS cm^{-1} (at 25 °C) supplied by the Millipore Simplicity-UV purification system (Merck, USA).

2.2. Methods

2.2.1. Wettability modification

Modification of the wettability of the quartz plate was employed using an esterification technique described in detail elsewhere [25]. In short, before the modification, the material surface was chemically cleaned to thoroughly remove organic contaminants. This was followed by esterification in 1-propanol (for 2 h) and 1-butanol and 1-octanol (for 4 h).

2.2.1.1. Contact angle measurements. The equilibrium contact angle of the liquid (water and RL solutions) on the glass surface was measured by a sessile drop method using the OCA 15 EC contact angle meter (DataPhysics Instruments GmbH, Germany). The images of 0.2 μL liquid droplets deposited on the plate surface were recorded for 5 min until the equilibrium value was reached and then analysed using the SCA 20 shape analysis software (DataPhysics Instruments GmbH, Germany). The reported contact angles are the average values of ten independent droplets per sample. Measurements were made in a saturated vapour atmosphere to reduce droplet evaporation. The water contact angle of the cleaned quartz was 6° ± 1°, and the contact angles for three plates modified by esterification were as follows: 34° ± 1°, 48° ± 1° and 80° ± 1°.

2.2.1.2. Surface tension measurements. The surface tension of the RL solutions was measured using the pendant drop method [26] with an OCA 15 EC goniometer (DataPhysics Instruments GmbH, Germany). A series of RL solutions with different concentrations was prepared in the range of 0–500 mg·dm^{-3}. The sample of the solution was placed in a 1750 TLL 500 μL gastight syringe (Hamilton, NV, USA) equipped with a blunt tip needle with a 2.11 or 1.65 mm outer diameter. According to the

recommendation by Song and Springer [27], the needle diameter was chosen based on the solution's surface tension. The syringe needle was placed in the glass cuvette filled with a small amount of measured solution to ensure a saturated vapour environment to minimise the droplet's evaporation. A droplet of the solution was then formed at the tip of a needle. The size of a pendant drop was adjusted to be large enough so its shape significantly differs from a spherical shape due to its own mass. Images of a droplet suspended from a needle were captured every 1 min for 60 min. This time was sufficient for the surface tension to reach equilibrium. The recorded sequence of images was then analysed with SCA20 software (DataPhysics Instruments GmbH, Germany) to obtain surface tension values. The software performs a numerical fitting process, which involves comparing the theoretical shape of a droplet predicted by the Young-Laplace equation with the recorded shape. Each dynamic surface tension curve was measured three times. The equilibrium value after 60 min was used as the surface tension value for a given rhamnolipid concentration.

2.2.1.3. Bubble motion in surfactant solution. To study the bubble behaviour in RL solution, a glass column with a square cross-section of 40x40 mm and a height of 260 mm was employed, along with a heavy-walled capillary with an internal diameter of 0.025 mm at the bottom (VitroCom, USA). The column was filled with water or RL aqueous solution, and a single bubble generator [28] was used to create an air bubble through the capillary. A high-speed camera (Optronis GmbH, Germany) equipped with a telecentric lens and illuminator (Sill Optics GmbH & Co. KG, Germany) was used to record images of the bubble at 1 ms intervals, 250 mm above the capillary orifice. The image resolution was 3.3 μm·pix^{-1}.

The recorded images were processed using MATLAB (MathWorks, USA) to extract variables of interest, such as bubble local rising velocity (v_b), calculated as

$$v_b = \frac{\sqrt{(x_{i+1} - x_i)^2 + (y_{i+1} - y_i)^2}}{t_{i+1} - t_i} \quad (1)$$

where $\times$ and y are vertical and horizontal coordinates of the geometrical centre of the bubble measured for two successive frames, and index I denotes the order of the image in the sequence. The time step ($t_{i+1} - t_i$) was 1 ms. In addition, the vertical (d_v) and horizontal (d_h) diameters of the bubble were determined to calculate the equivalent diameter of the bubble (d_b) and its deformation ratio (χ)

$$d_b = \left(d_h^2 \hat{A} \cdot d_v\right)^{\frac{1}{3}} \quad (2)$$

$$\chi = \frac{d_h}{d_v} \quad (3)$$

The reported values are the average of 30 independent measurements per surfactant concentration.

2.2.1.4. Bubble adhesion. The process of bubble-surface interaction was examined using the experimental setup described above in Section 2.2.4. For selected concentrations of RL, a quartz plate was mounted into a Teflon holder, which was then placed in the column 250 mm above the capillary orifice (Fig. 1).

Frame-by-frame analysis of the recorded image sequences of the colliding bubble was conducted to determine the TPC formation time (t_{TPC}), that is the period between the first bubble collision and the moment of TPC formation (moment of wetting film rupture). Therefore, t_{TPC} can be defined as the sum of the bubble bouncing time (t_b) and drainage time (t_d) of the liquid film [29]. Here, the bubble velocity and diameter were also determined according to equations E1 and E2 and the three-phase contact diameter (d_{TPC}), which was used to calculate the three-phase contact line expansion velocity (v_{TPC}) as

$$v_{TPC} = \frac{d_{TPC,\,i+1} - d_{TPC,\,i}}{t_{i+1} - t_i} \quad (4)$$

Furthermore, the captive bubble contact angle (θ_{CB}) during TPC line propagation and equilibrium was determined. Values of all determined parameters are reported as the average from 30 independent runs.

In the case of measurements where the formation of a three-phase contact was not observed within 30 s (this is the maximum recording time of the full measurement sequence) after the bubble collided with the surface, additional measurements were carried out with a lower time resolution that allowed the bubble to be observed under the surface of the solid for 5 min. All measurements were carried out in 1 mM NaCl background solutions.

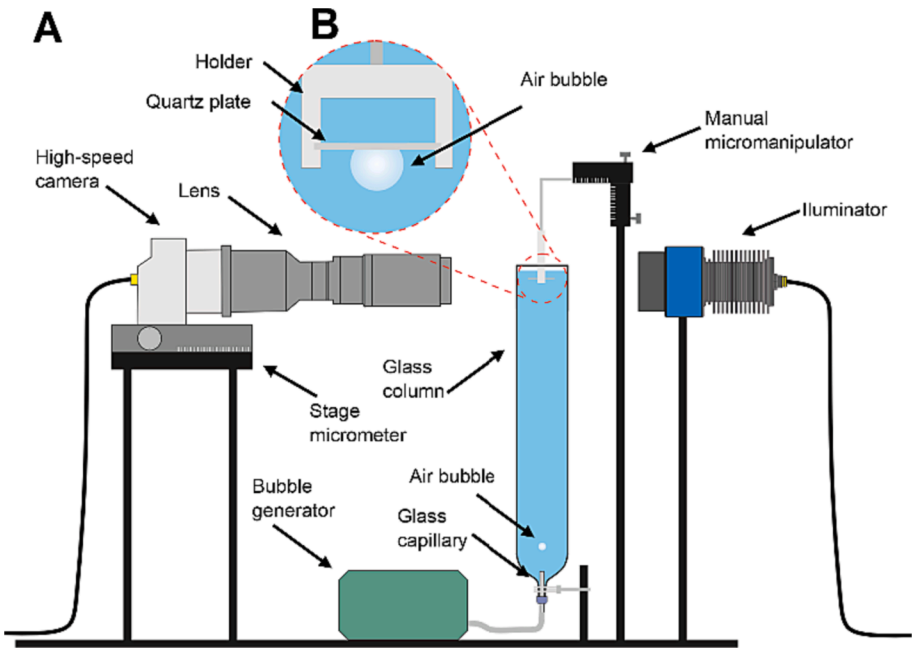

Fig. 1. Experimental setup for monitoring air bubble interactions with quartz surface (A). Side view (B) shows the mounted quartz plate with an adhered air bubble.

3. Results and discussion

3.1. Surface tension

The equilibrium surface tensions of aqueous solutions of RL at pH 5 and 10 plotted versus surfactant mass concentration are presented in Fig. 2. As can be observed, when the concentration exceeds 1 mg·dm^{-3}, the surface tension begins to decrease rapidly from 72.1 mN·m^{-1} to 32–33 mN·m^{-1} for both pH values, where the critical micelle concentration (CMC) is reached. This clearly indicates that RL has a very good ability to lower surface tension even at low concentrations. The CMC value of other RL mixtures may vary depending on the exact composition, which depends on the carbon source used. For the biosurfactant mixture tested, the CMC extracted from these plots was 26 mg·dm^{-3} at pH 5, while for pH 10, it was more than three times higher, equal to 90 mg·dm^{-3}. These values are within the range already reported for RL by other researchers [30,31].

Differences in the surface tension of the RL solution depending on the pH are the direct result of its molecular structure. The carboxyl group (–COOH) is sensitive to the pH of the solution, and depending on its value it can be in protonated (–COOH) or deprotonated form (–COO$^-$). The pK_a values (pH at which the molecule is 50% protonated) for mono- and di-RL reported by Abbasi and co-workers [32] were 5.5 and 5.6, respectively. According to their data, at pH 5, more than 90% of the molecules will be neutral. Differences in the ability of RL to change surface tension depending on the solution's pH and the molecule's structure were reported by Özdemir and co-workers [33]. In their study, they compared the surface and interfacial tensions of pure solutions of mono-RL and di-RL at the pH values of 5 and 6.8. At a pH of 6.8, most of the carboxyl groups dissociate to form carboxylate groups that confer anionic properties on the molecule (Fig. 3), while at pH 5, the protonated form is prevalent in the solution, giving the molecule non-ionic properties.

The results of Özdemir and co-workers [33] indicated that pH has the greatest impact on CMC and the minimum surface tension value of the rhamnolipid solution. These parameters were practically unaffected by the type of rhamnolipid, although mono-RL molecules exhibit higher surface activity at concentrations below the CMC. Also, the interfacial behaviour of mono- and di-RL molecules below the CMC differed significantly based on their interaction with the structure of the molecules at the interface. Specifically, mono-RL molecules demonstrated a

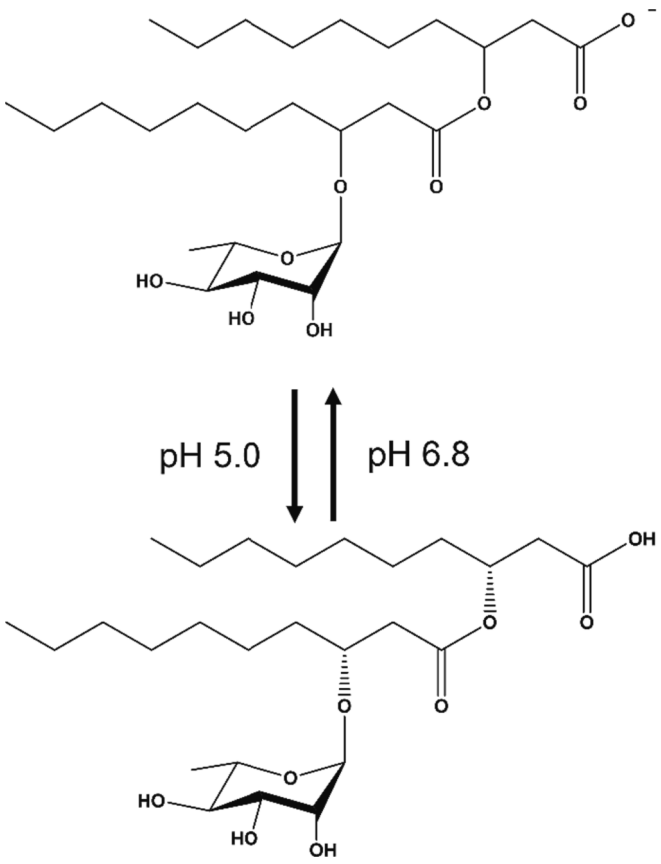

Fig. 3. Charge dependence of the rhamnolipid molecule (Rha-C_{10}-C_{10}) on the pH of the solution.

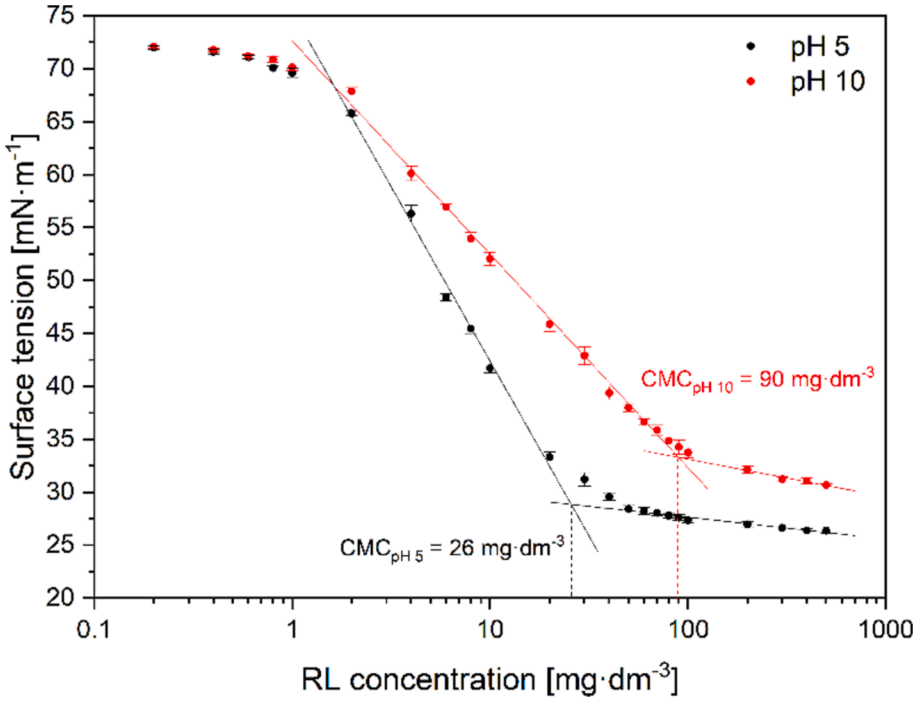

Fig. 2. Equilibrium surface tension of aqueous solutions of rhamnolipid at pH 5 and 10 as a function of mass concentration.

greater ability to reduce interfacial tension compared to those of di-RL molecules. The critical micellisation concentration at pH 5 was almost an order of magnitude lower than at pH 6.8, since at lower pH there is no electrostatic repulsion between the heads of the undissociated biosurfactant. Therefore, molecules can pack more tightly at the gas–liquid interface [34].

Hence, the values of pH chosen in this study were 5 for the non-ionic form and 10 for the anionic form. A pH of 10 was chosen since it is easier to set in a solution compared to lower values closer to 7. Furthermore, as there is no significant effect on the rhamnosyl group in this pH range, it remains unaltered [35]. Its dissociation occurs when the pH exceeds 11.

As stated by Özdemir and co-workers [33], stronger interactions between undissociated rhamnolipid molecules lead to increased compaction at the surface monolayer. Thus, we used our surface tension data to determine the minimal area (A_{min}) occupied by one molecule, as follows:

$$A_{min} = \frac{1}{N\hat{A}\cdot\Gamma_{max}} \quad (5)$$

where N is Avogadro's number, and Γ_{max} is the surface excess calculated using the equation [33,36]:

$$\Gamma_{max} = -\frac{1}{nRT}\hat{A}\cdot\frac{d\gamma}{dlnC} \quad (6)$$

where R is the gas constant (8.314 J·mol^{-1}·K^{-1}), T is the temperature (K), $d\gamma/d$lnC is the slope of the linear part of the surface tension vs the logarithm of concentration dependence, and n is a molecule-specific dissociation number. This number was taken as 1 at pH 5, assuming that RL is weakly ionised in these conditions. At pH 10, n was taken as 2 taking into account that most of the carboxyl groups of RL are deprotonated at this pH [33,37].

The calculated minimal surface area occupied by one molecule at pH 5 (Table 1) is much smaller than at pH 10. It is consistent with the assumption that, at lower pH, surfactant molecules can pack more closely at the interface and exhibit lower surface tension because of decreased electrostatic repulsion between carboxylate groups. These results demonstrate that RL self-assembly is most effective at the gas–liquid interface at pH 5. Furthermore, the hydroxyl groups of RL molecules at pH 5 can easily participate in hydrogen bonding interactions with water molecules [38,39].

3.2. Contact angle

Contact angle measurement is the basic technique used to quantify mineral surface wettability in flotation research, including in the presence of flotation reagents. High values of contact angles translate to highly hydrophobic surfaces, indicating a higher probability of adhesion between particles and bubbles [40]. The measured contact angles for the water and RL solutions are presented in Fig. 4. As can be seen, complete spreading of the RL solution was observed only in the case of a highly hydrophilic surface, with a water contact angle of 6°. Identical values were obtained for all biosurfactant concentrations. This shows that the biosurfactant does not cause hydrophobisation of the nonmodified quartz surface. In the case of esterified surfaces with higher hydrophobicities, the contact angle decreased marginally for low concentrations of RL. For a concentration <50 mg·dm^{-3}, the aqueous solution of rhamnolipid is a poor wetting agent, especially compared to its ability to lower surface tension (Fig. 2). Zdziennicka and Janczuk, who investigated the wetting properties of polytetrafluoroethylene, polyethylene and quartz with aqueous solutions of rhamnolipid and surfactin (up to 40 mg·dm^{-3}), also drew a similar conclusion on wetting properties of rhamnolipid [41].

Table 1
Surface tension, critical micelle concentration, and minimum surface area of RL at the gas–liquid interface at different pH values.

Property	pH 5	pH 10
CMC (mg·dm^{-3})	26	90
Surface tension at CMC (mN·m^{-1})	32.1	34.3
dγ/dlnC	−0,033	−0,021
A_{min} (Å^2·molecule $^{-1}$)	12	39

A distinct decrease in the contact angle value occurred in the vicinity of and beyond the CMC, where the surface tension reached almost the lowest values. The magnitude of the change in contact angle value was strictly dependent on the pH of the solution. The non-ionic form of RL (pH 5) caused a much greater reduction in the contact angle value compared to that of the anionic RL form (pH 10). The contact angle defined by Young's equation [42] depends on the liquid–gas, solid–gas and solid–liquid interfacial tensions. As this decrease is not the effect of changes in the gas–liquid interfacial tension above CMC, which, as mentioned above, reaches practically constant values, it must be the result of the adsorption of the surfactant on the solid surface modified by alcohol molecules.

For the adsorption of surfactants from an aqueous solution onto hydrophobic solid surfaces, the process mainly involves the adsorption of a hydrophobic chain of surfactant molecules onto a hydrophobic solid surface [43]. As the surfactant concentration in the solution rises, the increased packing of tails at the surface pushes the heads into the solution. As a result, the formation of an adsorption monolayer and even the formation of admicelles, i.e. aggregates in which hydrophobic chains create a non-polar environment on the surface of the solid, so the outer surface of the admicelles is ionic, can occur [44]. The concentration at which this phenomenon occurs is known as the critical surface aggregation concentration (CSAC) and is typically observed at around 60% of the CMC [45,46]. This suggests that for the indicated concentrations, the adsorption of rhamnolipid molecules must take place with their tails toward the alcohol-modified quartz surface and their heads towards the solution. As quartz possesses a significant negative zeta potential at pH 10, it is most likely the case that under these conditions, the adsorption of the ionic form of the surfactant is much lower than at pH 5 and its non-ionic form, which would also explain the lower ability of pH 10 solutions to lower the contact angle. As demonstrated by the research of Kruszelnicki and co-workers [47], the modification method used does not significantly alter the zeta potential of the silica surface, so it should be assumed that the examined hydrophobic surfaces also have a significant negative potential. For example, in the case of a quartz surface with a water contact angle of 80°, the use of a solution at a concentration of 100 mg·dm^{-3} and pH 5 resulted in a reduction in the contact angle value to 59°. Similarly, for pH 10, the angle was reduced to a value of 72°, while for the highest concentration used, the angle value decreased by 57° and 18°, respectively. Complete wetting of hydrophobic surfaces was not observed for any of the solutions studied.

On the other hand, the lack of ability of RL, used in low concentrations, to significantly decrease the value of the contact angle shows that RL does not negatively affect the hydrophobicity of the mineral surface, which has a positive meaning in the context of the bubble adhesion process and also the flotation itself.

3.3. Bubble motion in biosurfactant solution

In flotation, a variety of chemical compounds, both inorganic and organic, are used to control the properties of the phase interface. They are commonly divided into three main groups: collectors, frothers, and regulators [6]. From the perspective of bubble properties and their behaviour in solution, the greatest impact comes from the frothers. The primary objective of these modifications is to alter the properties of the liquid–gas interface in order to improve various critical factors that affect separation efficiency, such as the degree of gas dispersion, the inhibition of coalescence, the velocity of bubble rise, and the formation and stability of froth. Hence, the effect of RL on the behaviour of the bubble in solution was determined.

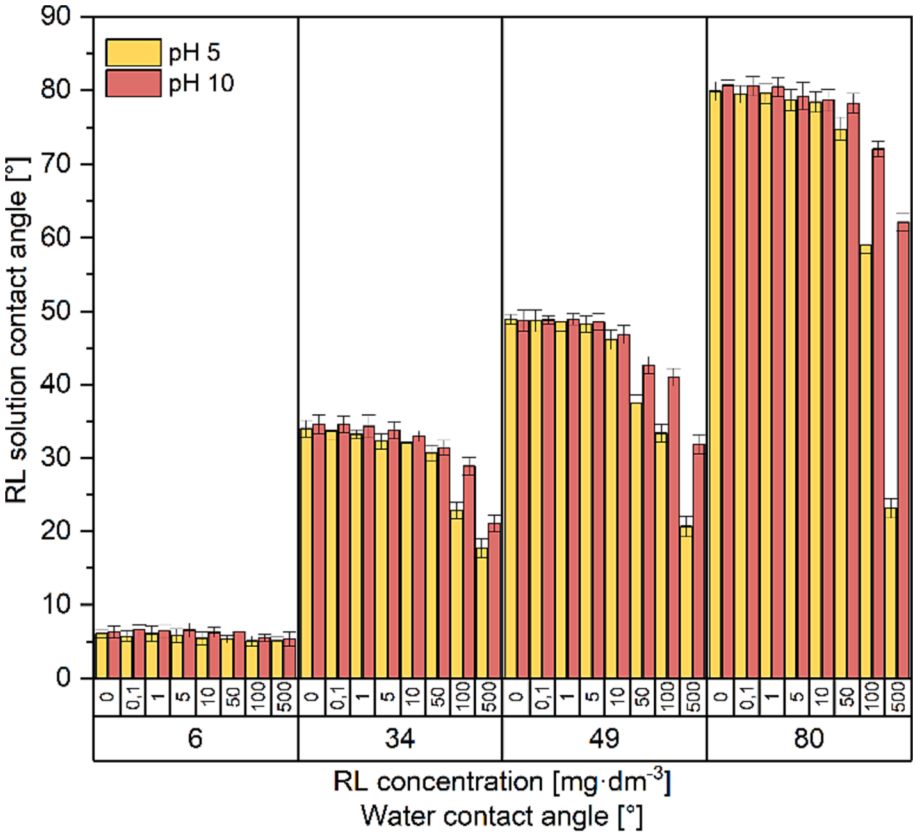

Fig. 4. Equilibrium contact angle of droplets of rhamnolipid solution of different concentrations and pH placed on the surface of quartz slides of different contact angles (values at 5 min after droplet deposition).

The values of the terminal velocity of the bubble (the constant value of bubble velocity determined by the balance between all the acting forces [48]) in water and the aqueous solutions of RL are presented in Fig. 5. It can be clearly seen that (as reported earlier for various surfactants) the terminal velocity of the bubble depends on the amount of surfactant in the liquid. Initially, the bubble surface is fully mobile for pure water, so its velocity and diameter are the highest possible and equal to 26.1 cm·s^{-1} and 996 μm, respectively. These values agree very

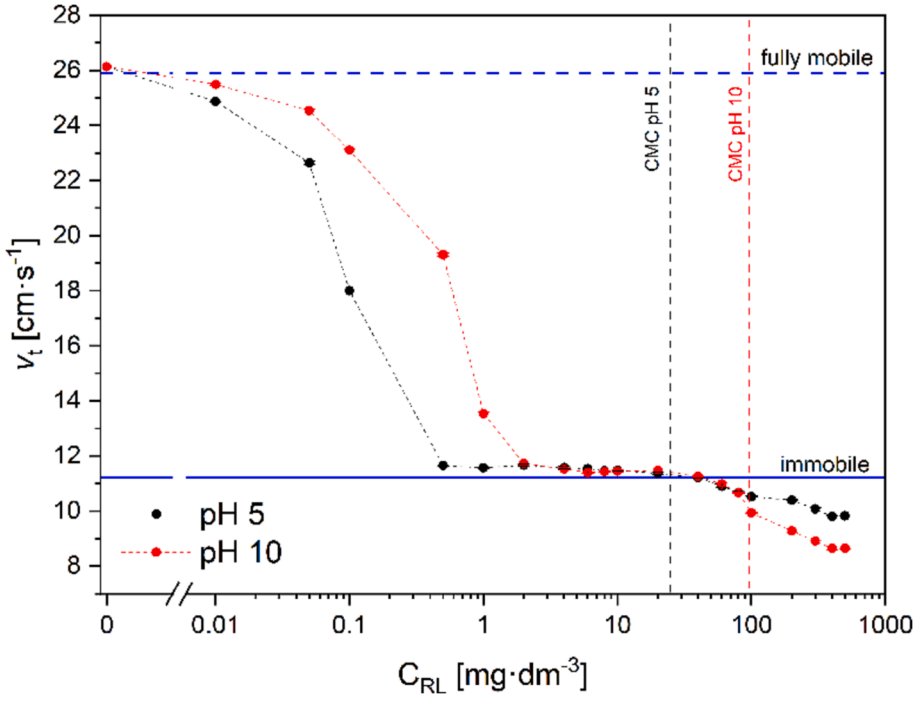

Fig. 5. Bubble terminal velocity as a function of RL concentration and pH.

well with the theoretical prediction of a model proposed by Manica et al. [49], presented in Fig. 4 as a dashed line (theoretical terminal velocity was calculated using $\gamma = 72.3$ mN·m^{-1}, liquid density $\rho = 998$ kg·m^{-3}, liquid viscosity $\mu = 1 \times 10^{-3}$ Pa·s and gravity constant $g = 9.81$ m·s^{-2}). As the concentration of the surfactant increases, the values of the terminal velocities decrease rapidly until they reach a minimum value of approximately 12 cm·s^{-1} at a concentration of RL 2 and 0.5 mg·dm^{-1} for pH 5 and 10, respectively, where the bubble surface is fully immobilised (and so-called steady-state conditions are reached). Such rapid velocity changes result from the fact that a gas bubble is extremely sensitive to any change in the surface tension of the liquid caused by the appearance of additional substances in the liquid, especially as a surface active agent. The solid line in Fig. 5 denotes the theoretical velocity of a bubble with a fully immobilised interface according to the classical Schiller-Naumann formula [50] for $\rho = 998$ kg·m^{-3}, $\mu = 1 \times 10^{-3}$ Pa·s and $g = 9.81$ m·s^{-2} and the bubble size equal to 996 μm. As seen, despite full immobilisation of the rising bubble surface after reaching threshold concentrations (2 and 0.5 mg·dm^{-1} for pH 5 and 10, respectively), a small but significant decrease of bubble velocity occurs at concentrations greater than ca. 30 mg·dm^{-3}. This effect was caused by the rapid decrease in bubble diameter observed for C_{RL} greater than 30 mg·dm^{-3}, down to 736 and 832 μm at pH 5 and 10 respectively for the highest concentration of 500 mg·dm^{-3} (Fig. 6A), and will be discussed below.

The bubble's movement and surface mobility depend on the presence of surface-active substances in the liquid. The effect of surfactant concentration on the bubble is complex and is influenced by various factors such as surface activity, gradients in surface tension, the orientation of surface active molecules, and their packing at the interface. The bubble's surface is free from surfactants in pure water, giving it high mobility. Therefore, the bubbles take the shape of an ellipse. In this case, the deformation coefficient, which is the ratio of the horizontal to the vertical diameter of the bubble, takes values greater than one (while a value of 1 indicates a spherical geometry). It is well known that when a bubble moves in a liquid containing a surfactant, its molecules accumulate at the gas–liquid interface, creating an adsorption layer. As the bubble rises in a continuous medium, viscous drag causes the adsorbed molecules to be carried to the bottom of the bubble surface, resulting in an accumulation of surfactant molecules and an unequal distribution of surface tension. This type of adsorption layer is known as a dynamic adsorption layer (DAL) [51]. The presence of a coverage gradient induces Marangoni effects that counteract the shear flow and ultimately leads to the immobilization of the bubble surface. That is why for highly concentrated surfactant solutions, bubbles behave like a rigid sphere, and the reduction of their velocity is significant [52,53].

As can be seen from Fig. 6A, the presence of the surfactant in concentrations below CMC did not affect the equivalent diameter of the bubble, while there was immobilisation of its surface, revealed by a decrease in the value of the deformation coefficient, that is, the ratio of horizontal to vertical diameter (Fig. 6A). Comparison of the values of the deformation coefficient for the given concentrations at pH 5 and 10 confirms that the non-ionic form of rhamnolipid has a greater ability to accumulate on the bubble surface, as a more surface active compound (see Fig. 2).

Interestingly, as seen in Fig. 6B, a decrease in the bubble velocity, observed for C_{RL} greater than 20–30 mg·dm^{-3}, can be associated with the bubble size decrease – experimental data follow the trend shown by the Schiller-Naumann model (solid line in Fig. 6B) [50]. However, a clear discrepancy from the model predictions arises with bubble size decrease. The direction of this difference depends on the charge of the RL molecules in the solution. For pH = 10, lower bubble velocity can be explained by a slight increase in the solution viscosity associated with bulk micelle formation. On the other hand, at pH 5, an observed increase in the bubble velocity (increase in surface mobility) may occur when molecules desorb faster from the interface [54].

3.4. Three-phase contact formation

The variation in the TPC formation time values in the single bubble experiment is presented in Fig. 7. Generally there are two mechanisms of a wetting film rupture related to (i) electrostatic interactions between interfaces of a solid substrate and a gas bubble (characteristic for hydrophilic and slightly hydrophobic surfaces, so-called capillary waves or spinodal dewetting), and (ii) nucleation mechanism at solid substrates of enough degree of hydrophobicity. As was shown in the literature, with increasing degree of solid surface hydrophobicity, the former mechanism is gradually shifted towards the latter [55–58]. As can be seen in the case of the highly hydrophilic quartz surface ($\theta = 6°$), no bubble adhesion was observed regardless of the concentration of the surfactant and pH of the solution. The presence of RL did not cause destabilisation of the thin film. The contact angle value was too small for a thin film rupture to occur. A lack of three-phase contact formation was also observed for a plate with a contact angle of 34° at pH 10 under conditions where the RL molecules were in the anionic form. The stability of thin wetting films on hydrophilic solid surfaces depends primarily on the electrostatic interactions between the interfaces [55]. The pH of the solution heavily influences the nature of ions adsorbed onto a solid

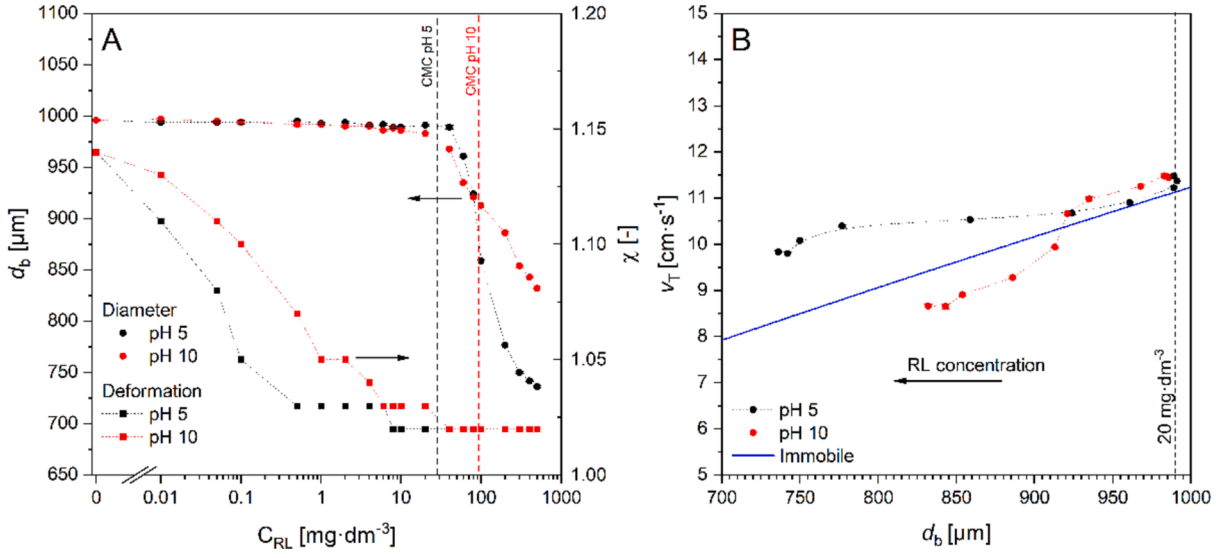

Fig. 6. Bubble diameter (d_b) and deformation (χ) as a function of RL concentration (A) and bubble terminal velocity as a function of its diameter (B).

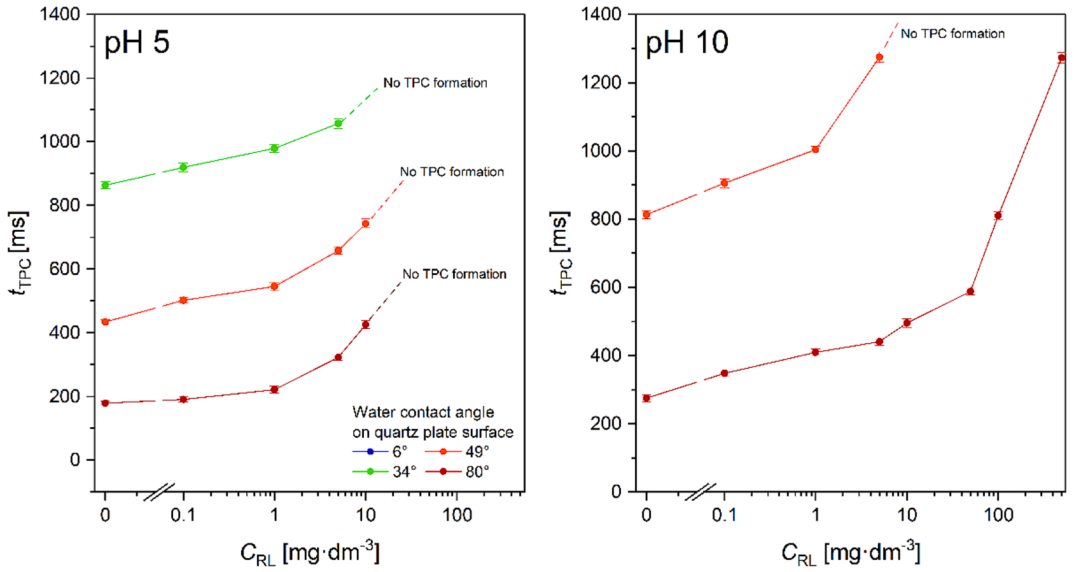

Fig. 7. Value of t_{TPC} as a function of RL concentration for examined solid surfaces at pH 5 and 10.

surface. The quartz surface immersed in an aqueous phase exhibits a negative charge across almost the entire pH range (pH_{iep} 2–3) [59]. Similarly, the air bubble carries a negative charge in a wide pH range (pH_{iep} 3–4) [60]. Thus, in this case, the degree of surface hydrophobicity was too small to overcome the repulsive electrostatic forces stabilising the thin film resulting from the interaction of negatively charged surfaces and to trigger the nucleation mechanism of film rupture.

In conditions where degree of hydrophobicity was sufficient for TPC to form (i.e. when the contact angle of the solid surface was high enough for the nucleation mechanism to come to play), it can be seen that for low concentrations of surfactant, the TPC formation time was not significantly different from the values obtained for water. For concentrations up to 1 mg·dm^{-3}, the difference did not exceed 200 ms. An increased concentration caused an extension of the TPC formation time. This indicates that the film showed higher stability. For example, in the case of the surface with $\theta = 80°$, the t_{TPC} was extended from 275 ± 10 ms in pure water to 1273 ± 15 ms in 500 mg·dm^{-3}. However, there are also observable thresholds for the concentration of RL beyond which the t_{TPC} values begin to increase significantly. This was especially apparent in the case of the anionic form. In addition, when the concentration reached a high enough value, the three-phase contact no longer formed. This effect was especially noticeable at pH 5, that is, for RL in non-ionic form. The concentration value above which adhesion was no longer observable was 5 mg·dm^{-3} for surfaces with a contact angle of 34° at pH 5 and 49° at pH 10 and 10 mg·dm^{-3} for $\theta \geq 49°$ at pH 5.

The variable t_{TPC} is the sum of the bubble bouncing time (t_b) and the thin film drainage time (t_d). Fig. 8 presents a sequence of images showing the phenomenon occurring during bubble interaction with a quartz surface with $\theta = 80°$ in 1 mg·dm^{-3} RL solution of pH 10. The moment of the first collision was set as the time of 0 ms.

The prolongation of three-phase contact formation time with increasing concentration is clearly the effect of the increase in film

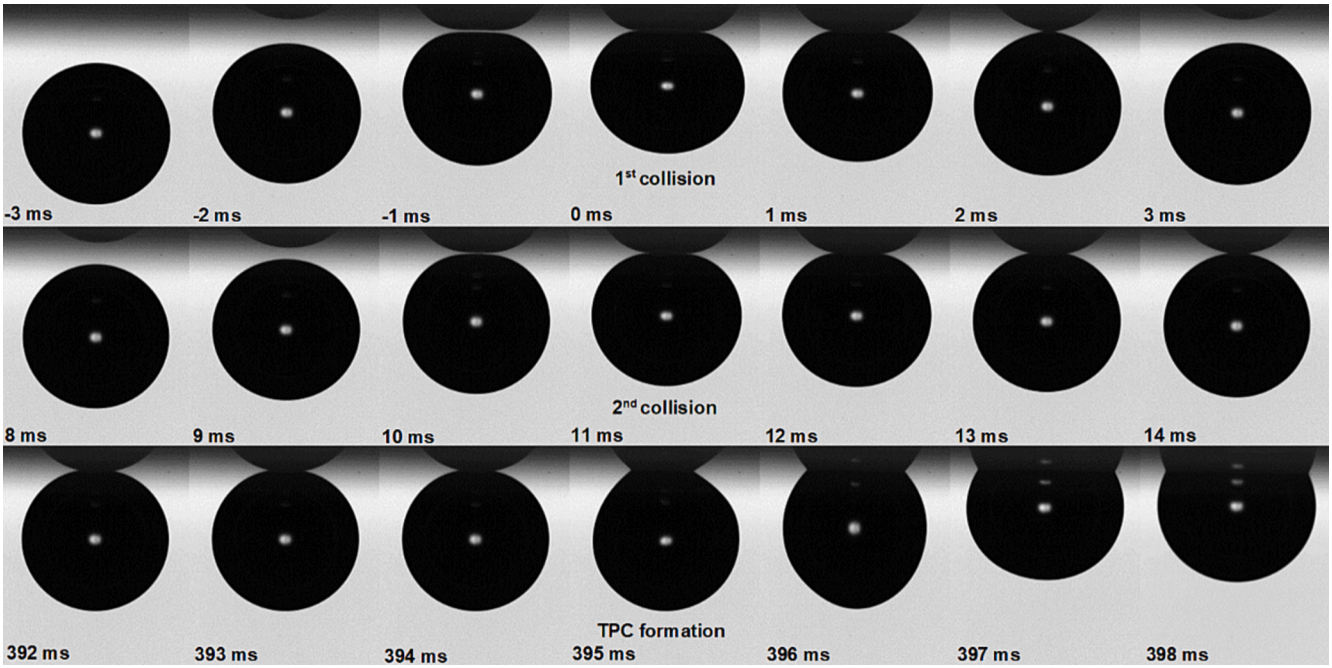

Fig. 8. Sequences of images of a bubble colliding with a quartz plate ($\theta = 80°$) in 1 mg·dm^{-3} RL solution of pH 10.

drainage time, as can be seen in Fig. 9. The bouncing time, on the other hand, decreased, resulting mainly from a lower bubble impact velocity (Fig. 5), which strongly affects the bouncing stage of bubble-surface interaction [61]. The number of bubble rebounds decreased from three for water to zero for a concentration of 10 mg·dm^{-3}, i.e. when the terminal velocity decreased from 25.6 to 11.1 cm·s^{-1}. A reduction in bubble diameter to 989 and 986 μm at pH 5 and 10, respectively, was also observed. However, the decrease in bounce time was not as significant as the increase in the drainage time of the film formed on surfaces of different hydrophobicity values in its effect on the total contact formation time. Therefore, an increase in t_{TPC} was observed, as mentioned above.

The increase in the drainage time of the thin film ~~is~~ observed with increasing rhamnolipid concentration can be associated with (i) greater wetting of the surface by the solution, as demonstrated by the contact angle measurements shown in Fig. 4 and discussed in section 3.2, as well as (ii) increase in degree of the bubble surface immobilization with increasing RL concentration (see discussion associated with Fig. 5). The aforementioned higher ability of the non-ionic rhamnolipid solution to wet the surface, in effect, resulted in the inability of TPC formation for a concentration above 10 mg·dm^{-3}. On the other hand, at pH 10, the effect of the surfactant on hydrophobic silica surface wettability was much lower compared to pH 5; hence the three-phase contact formed for higher concentrations.

The ability of this biosurfactant to form stable foam films will undoubtedly play a role in this effect. As Cohen and co-workers [62,63] observed in their study, the foam films created by RL solutions show high stability in this concentration range. The increase in the concentration of RL in the solution obviously contributed to an increase in bubble coverage (gas/liquid interface), which resulted in slower film drainage. Also, Khoshdast and co-workers [64] investigated the frothing and surface activity of the RL biosurfactant and compared the results with conventional flotation frothers, that is, methyl isobutyl carbinol (MIBC). Their results showed that RL exhibits much better surface activity, which means that it has a higher ability to lower surface tension. This was explained by the fact that it has a much higher molecular weight than typical foaming agents and a higher number of multiple oxygenated groups in its structure. According to the research, the oxygenated units in the RL structure can bond with water molecules via hydrogen bonding, which leads to the molecules adopting a flat orientation on the surface and possibly increasing the viscosity of the liquid film. In addition, they performed an elasticity calculation of the foam film formed by the reagents studied. Their results showed that the film formed with the use of RL has significantly higher elasticity and, thus, durability. The high molecular weight of biosurfactant molecules leads to a more viscous and hence more stable wetting film.

3.5. Three-phase contact line expansion

After the thin film rupture, the expansion of the three-phase contact line begins. For an efficient flotation process to take place, such factors as a high adhesion velocity of the bubble to the solid surface and high contact angles are required. The dynamics of TPC line propagation are affected by degree of surface hydrophobicity and the solid–liquid and liquid–gas interfacial tensions, which are, in turn, dependent on surfactant concentration. Changes in bubble shape during the movement of the gas–liquid interface cause variations in surfactant concentration and, therefore, the formation of its gradient, which induces Marangoni flow along the bubble surface, resulting in an interfacial gradient of surface tension [65].

To evaluate the effect of the presence of the biosurfactant on bubble adhesion, we determined the three-phase contact propagation velocities and the values of the contact angle during TPC expansion and when the equilibrium was reached.

3.5.1. TPC diameter

The calculated values of diameters of the TPC perimeters are illustrated in Fig. 10. Because the bubble diameter was reduced with increasing surfactant concentration, to evaluate the effect of its presence on the size of the three-phase contact formed, the d_{tpc}/d_b ratio was evaluated. The moment when the thin liquid film ruptured was set as zero time, and afterwards, an expansion of the TPC line was observed. The non-zero values of the TPC diameter before zero time result from inability of the image analysis technique to differentiate the thin liquid film between the bubble and the solid surface. Therefore, these values should be considered not to have any physical meaning [66].

As can be seen in Fig. 10, the expansion of TPC was increasing in time, and the rate of reaching the maximum value depended on the concentration of RL for a given degree of surface hydrophobicity. The process of bubble adhesion in pure water leads to the formation of the largest TPC perimeter, regardless of the surface's hydrophobicity. Also, for small concentrations of RL (<5 mg·dm^{-3}), the formation rate of a stable three-phase contact and equilibrium diameter does not differ significantly from the process occurring in pure water. The stable perimeter of the TPC line (the equilibrium value of the d_{TPC}/d_b ratio) is reached within a few milliseconds, particularly already after 5 ms. In the presence of the surface active substance, the kinetics of TPC line propagation are significantly affected. The effect of the surfactant becomes apparent at higher concentrations, causing an increase in the time required for the bubble to reach a stable position and also a decrease in the total area of contact between the bubble and the surface, which will certainly have a negative effect on actual flotation.

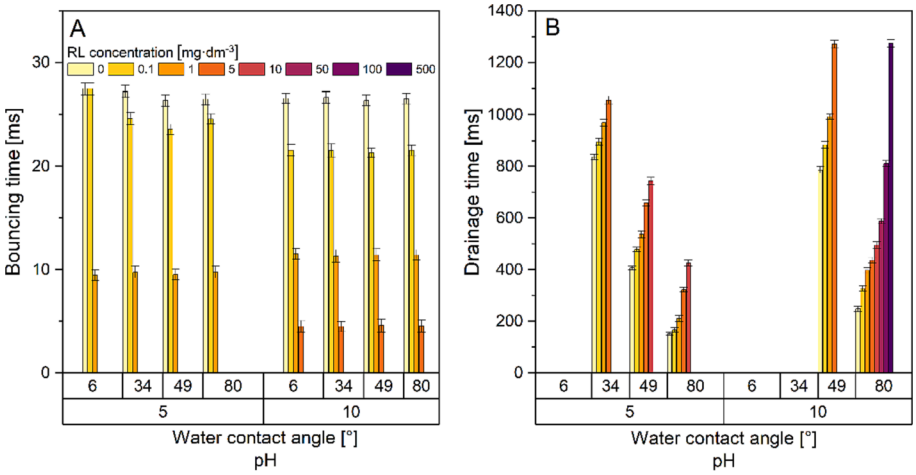

Fig. 9. Values of t_B (A) and t_D (B) as a function of rhamnolipid concentration for the examined solid surfaces at pH 5 and 10.

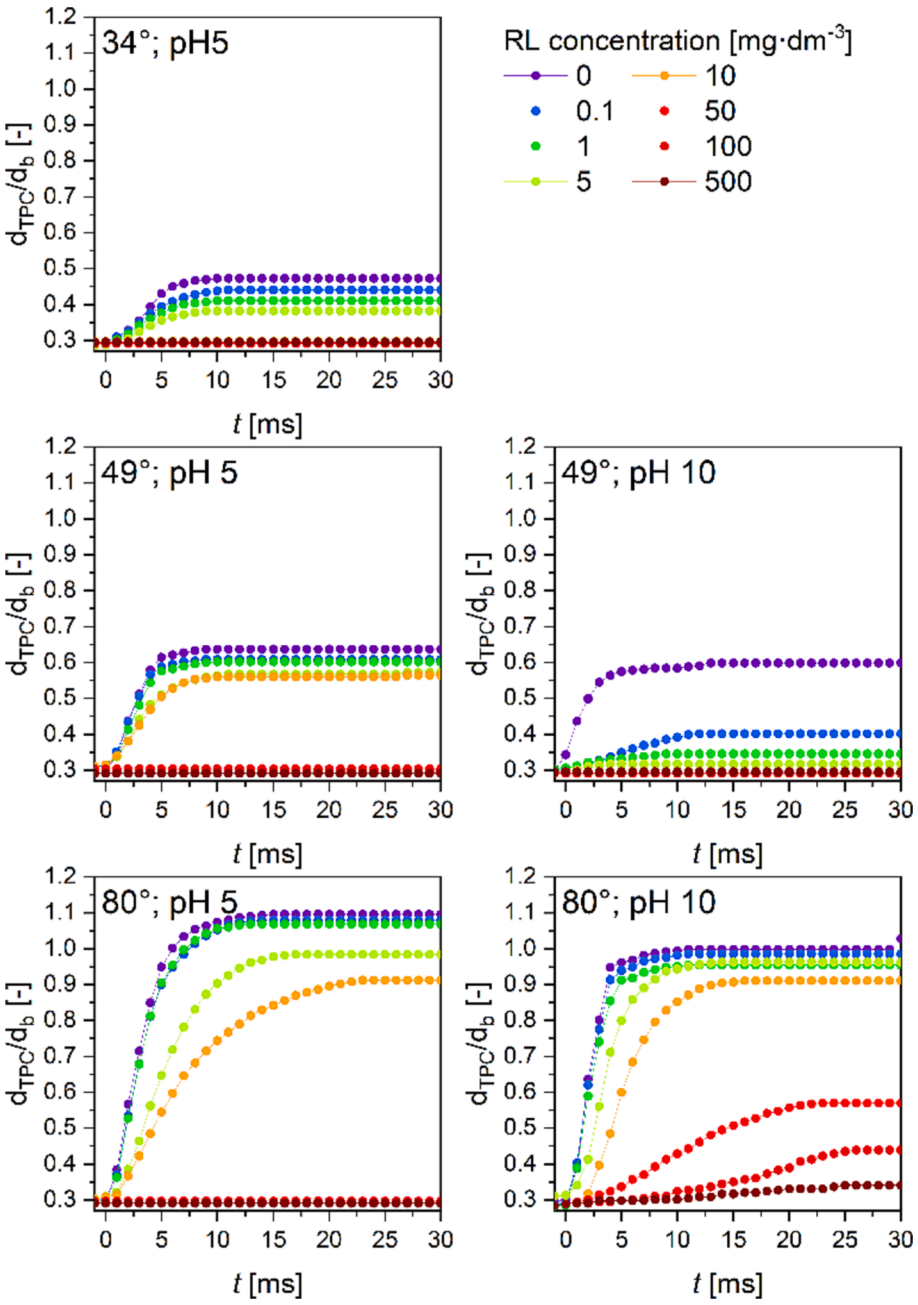

Fig. 10. Values of d_{TPC}/d_b ratio for bubble adhesion to the surface of different contact angles in rhamnolipid solution of pH 5 and 10.

3.5.2. TPC propagation velocity

The calculated values of three-phase contact line expansion velocities are given in Fig. 11. As can be seen, after the thin film rupture, the TPC expansion velocity increased in time, reaching a maximum and then gradually decreasing to low values. This pattern of contact line propagation has been previously reported by Basarova and co-workers [66,67]. Their study examined the TPC line expansion process during bubble adhesion onto hydrophobic surfaces in solutions of non-ionic surface-active agents of different structures (Terpineol, Triton X-100, and pentaethylene glycol monodecyl ether). They found that for a surfactant whose molecule has a long and flexible hydrophobic tail, bubble adhesion is very slow in solutions with concentrations close to or higher than the CMC. In our case, the maximum propagation velocity of TPC was observed for bubble adhesion in pure water, and its value decreased as the concentration of RL increased. Obviously, the additional key factor, in this case, was the hydrophobicity of the solid's surface itself. The higher the concentration was, the higher were the velocities reached for the corresponding concentrations. For the lowest contact angles of the solid surface for which the formation of three-phase contact occurred (i.e. 34° for pH 5 and 49° for pH 10), the velocities were extremely low (<5 cm·s^{-1}).

3.5.3. Bubble-solid contact angle

When the adhesion of a bubble to the surface of a solid is considered, the adhesion efficiency can be expressed by the value of the equilibrium contact angle between the air bubble and the solid. This parameter is an important characteristic of the flotation system. Similarly to the velocity of three-phase contact propagation, it depends on the degree of surface hydrophobicity and interfacial tension. The determined values of dynamic bubble contact angles are given in Fig. 12. In all experiments where a three-phase contact was established, the dynamic contact angle was found to increase from an initial value of zero (in the figure, it is a

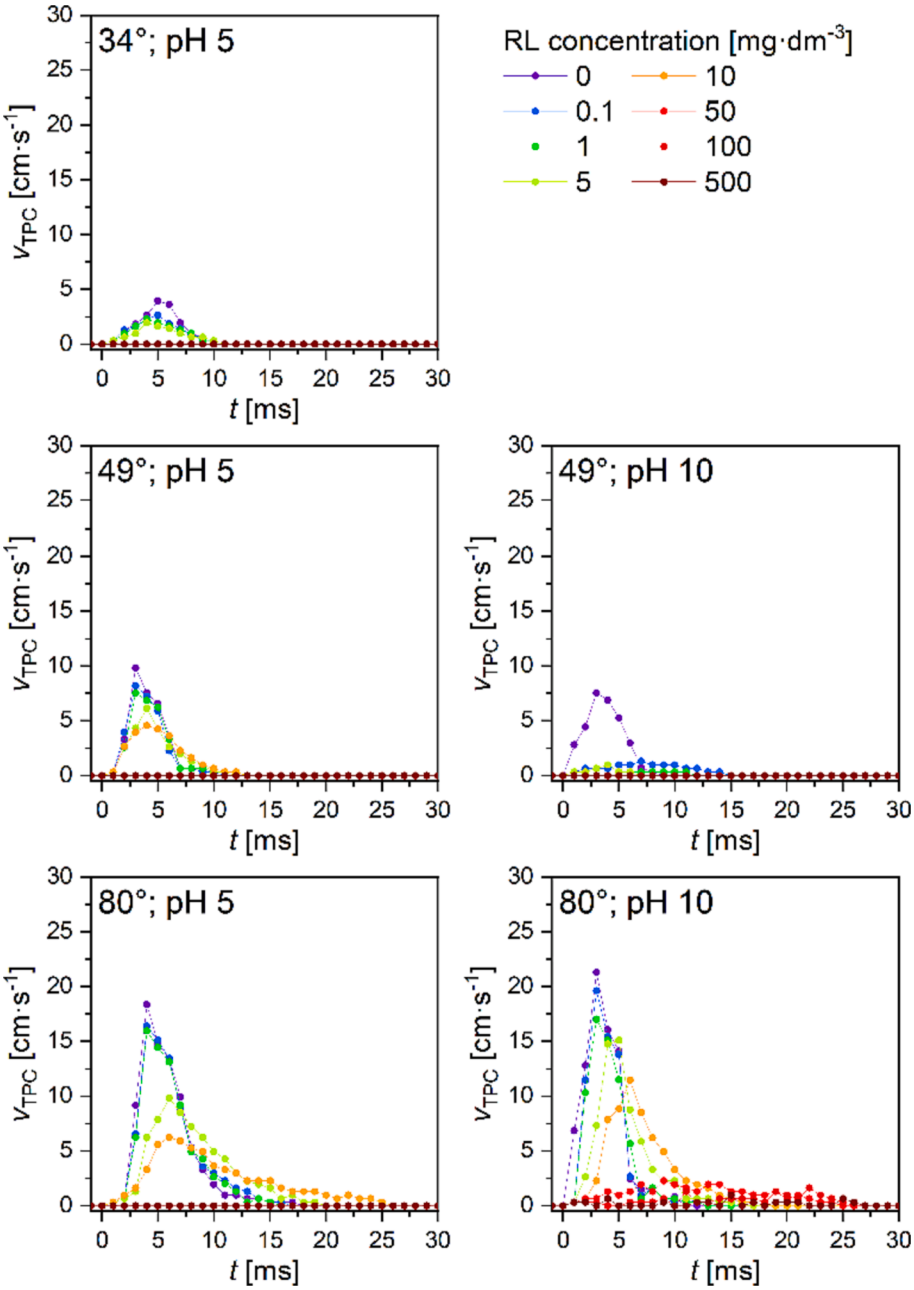

Fig. 11. Velocity of three-phase contact line expansion at the surface of different contact angles in rhamnolipid solution of pH 5 and 10.

value of 10° due to the analysis technique mentioned above) to an equilibrium value over time, and this time dependence was dependent on the concentration of the surfactant present. After reaching the equilibrium, the highest contact angle value is found for adhesion in pure water. This is due to the high surface tension of this liquid. As the concentration of the surfactant increases, the surface tension decreases, as does the equilibrium contact angle. At pH 10 for concentrations greater than 50 mg·dm^{-3}, contact angles are significantly lower than in pure water. Changes in the value of the dynamic wetting angle occurred more slowly over time.

4. Conclusion

The rupture of the thin liquid film separating the bubble and the solid surface is a crucial condition for the formation of the three-phase contact and the formation of an aggregate. The obtained results indicated that the three-phase contact formation time strictly depends on the concentration of RL biosurfactant. The time required to form a three-phase contact between a bubble and a quartz surface of various degrees of hydrophobicity was prolonged with the increase in the concentration of RL. Additionally, while rhamnolipid is non-ionic, particle-bubble adhesion can be inhibited when the surfactant concentration is too high. The leading cause of this effect was the high foaming power of the RL, which increased the stability of the thin liquid film formed between the bubble and the surface of the solid.

The study showed that in the case of RL, the key parameter is the pH of the solution, which determines whether the molecule assumes an anionic (pH 10) or non-ionic character (pH 5). The key distinction between the ionic and non-ionic forms of RL molecules lies in their ability to stabilise the thin film. The ionic forms exhibit much lower surface coverage and higher surface mobility as a result of the strong electrostatic repulsion between the charged surfactant molecules. On the other hand, the non-ionic molecules are capable of extensive coverage of the bubble surface, stabilising the foam films. Additionally, hydroxyl groups

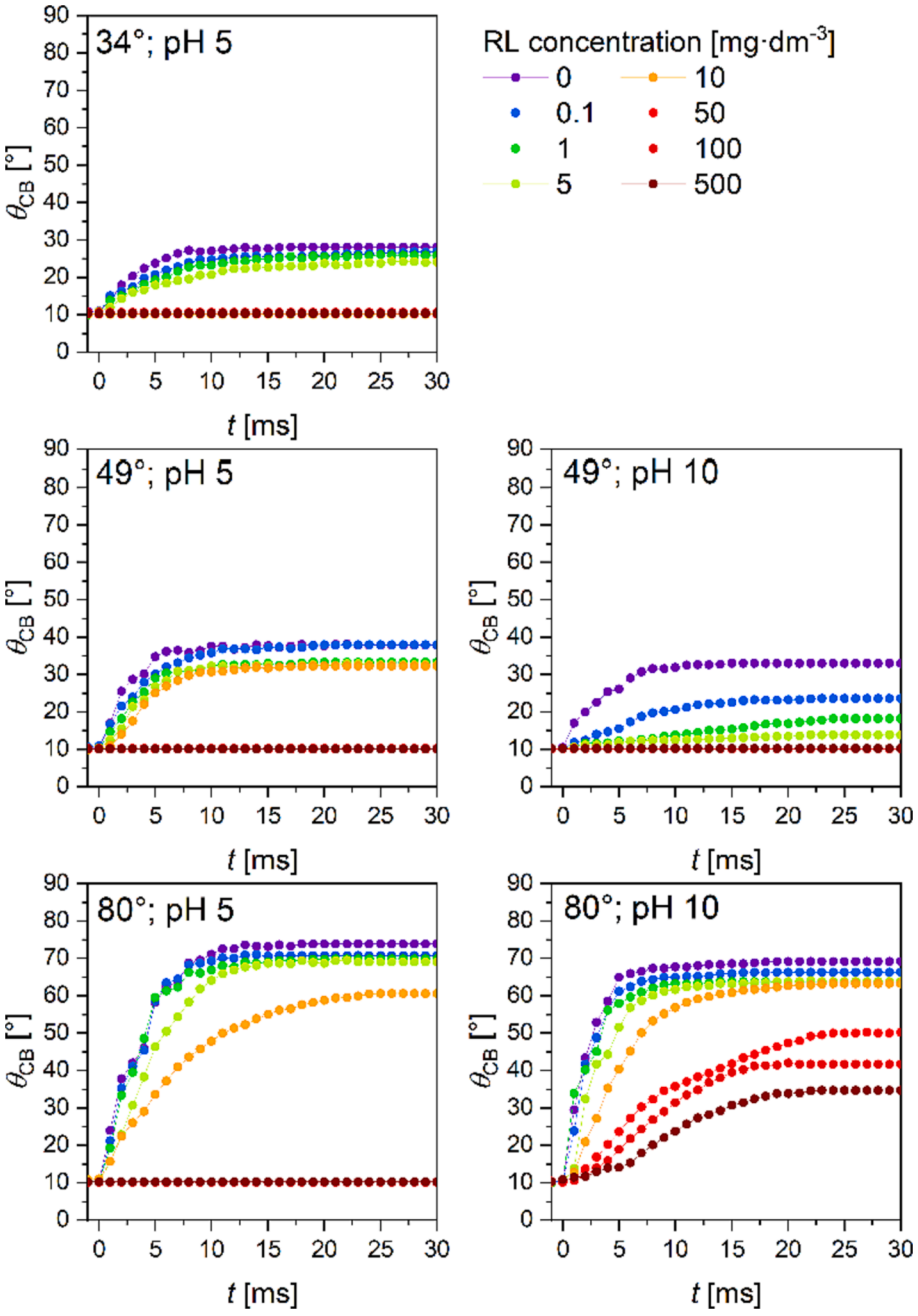

Fig. 12. Dynamic bubble contact angle during bubble adhesion on the surface of different contact angles in rhamnolipid solution of pH 5 and 10.

of non-ionic RL molecules are able to create hydrogen bonds with water molecules, which will form a hydration shell around the bubble. The factors outlined above also affect the bubble's mobility. The presence of the surfactant immobilizes the bubble surface, causing a decrease in velocity and changes in bubble size and shape, although deviations from theoretical model predictions. At this point, we are unable to provide an exact explanation for these deviations; therefore it requires further research.

In addition to the increase in the time required for the thin film to break and form a three-phase contact itself, in each case, the increasing concentration of rhamnolipid caused the three-phase contact perimeter to propagate more slowly. The size of the contact area between the bubble and the surface decreased, as did the value of the arising contact angle.

The prolongation of the three-phase contact formation time caused by the presence of RL in the solution will be of particular importance for the actual flotation process, in which this biosurfactant would be used as a collector or frothing agent. In such a case, especially at excessively high concentrations, it would have a negative impact on flotation kinetics and, thus, efficiency. This is especially true in excessively high concentrations. Hence, from a particle flotation point of view, rhamnolipid seems to be an unsuitable agent when used in an excessively high concentration because of its strong foaming action. On the other hand, as other studies have indicated, it shows very promising potential for use in ion flotation, where the interaction between rhamnolipid anions results in the formation of ionic clusters that are then removed by attaching to rising bubbles.

CRediT authorship contribution statement

Krzysztof Jan Legawiec: Conceptualization, Investigation, Project administration, Writing - original draft. **Mateusz Kruszelnicki:**

Conceptualization, Investigation, Methodology, Software, Writing – original draft, Resources, Data curation, Funding acquisition. **Michalina Zawadzka:** Investigation, Methodology. **Pavlína Basařová:** Investigation, Supervision. **Jan Zawala:** Writing – original draft. **Izabela Polowczyk:** Supervision, Writing - review & editing.

Declaration of Competing Interest

The authors declare that they have no known competing financial interests or personal relationships that could have appeared to influence the work reported in this paper.

Data availability

Data will be made available on request.

Acknowledgement

This study was financed by National Science Centre (Poland) Research Grant No. 2019/33/N/ST8/03026.

Appendix A. Supplementary data

Supplementary data to this article can be found online at https://doi.org/10.1016/j.molliq.2023.122759.

References

[1] A. Nguyen, H.J. Schulze, Colloidal Science of Flotation. 1 st, CRC Press, Boca Raton, 2003. 10.1201/9781482276411.
[2] H.J. Schulze, Hydrodynamics of Bubble-Mineral Particle Collisions, Miner. Process. Extr. Metall. Rev. 5 (1989) 43–76, https://doi.org/10.1080/08827508908952644.
[3] Y. Xing, M. Xu, X. Gui, Y. Cao, M. Rudolph, H.J. Butt, M. Kappl, The role of surface forces in mineral flotation, Curr Opin Colloid, Interface Sci. 44 (2019) 143–152, https://doi.org/10.1016/J.COCIS.2019.11.005.
[4] Y. Xing, X. Gui, L. Pan, B. el Pinchasik, Y. Cao, J. Liu, M. Kappl, H.J. Butt, Recent experimental advances for understanding bubble-particle attachment in flotation, Adv. Colloid Interface Sci. 246 (2017) 105–132, https://doi.org/10.1016/J.CIS.2017.05.019.
[5] P.B. Kowalczuk, J. Zawala, D. Kosior, J. Drzymala, K. Malysa, Three-Phase Contact Formation and Flotation of Highly Hydrophobic Polytetrafluoroethylene in the Presence of Increased Dose of Frothers, Ind. Eng. Chem. Res. 55 (2016) 839–843, https://doi.org/10.1021/ACS.IECR.5B04293.
[6] S.M. Bulatovic, Classification of Flotation Reagents, in: Handbook of Flotation Reagents, Elsevier, 2007, pp. 1–3, https://doi.org/10.1016/B978-044453029-5/50010-1.
[7] C. Nikolova, T. Gutierrez, Biosurfactants and Their Applications in the Oil and Gas Industry: Current State of Knowledge and Future Perspectives, Front. Bioeng. Biotechnol. 9 (2021) 46, https://doi.org/10.3389/FBIOE.2021.626639/BIBTEX.
[8] A. Pattanaik, R. Venugopal, A. Pattanaik, R. Venugopal, Role of Surfactants in Mineral Processing: An Overview, Surfactants and Detergents. (2019), https://doi.org/10.5772/INTECHOPEN.85947.
[9] E.S. Lakatos, L.I. Cioca, A. Szilagyi, M.G. Vladu, R.M. Stoica, M. Moscovici, A Systematic Review on Biosurfactants Contribution to the Transition to a Circular Economy, Processes 10 (2022) 2647, https://doi.org/10.3390/PR10122647.
[10] T. Ivanković, J. Hrenović, Surfactants in the environment, Arhiv za Higijenu Rada i Toksikologiju 61 (2010) 95–110, https://doi.org/10.2478/10004-1254-61-2010-1943.
[11] M.A.D. de Rienzo, P.J. Martin, Effect of Mono and Di-rhamnolipids on Biofilms Preformed by Bacillus subtilis BBK006, Curr. Microbiol. 73 (2016) 183–189, https://doi.org/10.1007/S00284-016-1046-4/FIGURES/4.
[12] A. Bodagh, H. Khoshdast, H. Sharafi, H. Shahbani Zahiri, K. Akbari Noghabi, Removal of Cadmium(II) from Aqueous Solution by Ion Flotation Using Rhamnolipid Biosurfactant As an Ion Collector, Ind. Eng. Chem. Res. 52 (2013) 3910–3917, https://doi.org/10.1021/IE400085T.
[13] W. Peng, L. Chang, P. Li, G. Han, Y. Huang, Y. Cao, An overview on the surfactants used in ion flotation, J. Mol. Liq. 286 (2019), 110955, https://doi.org/10.1016/J.MOLLIQ.2019.110955.
[14] A. Salmani Abyaneh, M.H. Fazaelipoor, Evaluation of rhamnolipid (RL) as a biosurfactant for the removal of chromium from aqueous solutions by precipitate flotation, J. Environ. Manage. 165 (2016) 184–187, https://doi.org/10.1016/J.JENVMAN.2015.09.034.
[15] V. Shojaei, H. Khoshdast, Efficient chromium removal from aqueous solutions by precipitate flotation using rhamnolipid biosurfactants, Physicochemical Problems of Mineral Processing. 54 (2018) 1014–1025, https://doi.org/10.5277/PPMP18103.
[16] D.E. Hogan, R.M. Stolley, C. Boxley, M.K. Amistadi, R.M. Maier, Removal of uranium from contaminated groundwater using monorhamnolipids and ion flotation, J. Environ. Manage. 301 (2022), 113835, https://doi.org/10.1016/J.JENVMAN.2021.113835.
[17] D.E. Hogan, J.E. Curry, R.M. Maier, Ion Flotation of La3+, Cd2+, and Cs+ using Monorhamnolipid Collector, Colloids and Interfaces 2 (2018) 43, https://doi.org/10.3390/COLLOIDS2040043.
[18] M. Mahmoodabadi, H. Khoshdast, V. Shojaei, Efficient Dye Removal from Aqueous Solutions Using Rhamnolipid Biosurfactants by Foam Flotation, Iranian Journal of Chemistry and Chemical Engineering (IJCCE). 38 (2019) 127–140. 10.30492/IJCCE.2019.37644.
[19] V.L. da Silva, G. Dilarri, C.R. Mendes, R.B. Lovaglio, A.R. Gonçalves, R. N. Montagnolli, J. Contiero, Rhamnolipid from Pseudomonas aeruginosa can improve the removal of Direct Orange 2GL in textile dye industry effluents, J. Mol. Liq. 321 (2021), 114753, https://doi.org/10.1016/J.MOLLIQ.2020.114753.
[20] T. Rasheed, S. Shafi, M. Bilal, T. Hussain, F. Sher, K. Rizwan, Surfactants-based remediation as an effective approach for removal of environmental pollutants—A review, J. Mol. Liq. 318 (2020), 113960, https://doi.org/10.1016/J.MOLLIQ.2020.113960.
[21] X. Long, G. Zhang, L. Han, Q. Meng, Dewatering of floated oily sludge by treatment with rhamnolipid, Water Res. 47 (2013) 4303–4311, https://doi.org/10.1016/J.WATRES.2013.04.058.
[22] H. Khoshdast, A. Sam, Z. Manafi, The use of rhamnolipid biosurfactants as a frothing agent and a sample copper ore response, Miner. Eng. 26 (2012) 41–49, https://doi.org/10.1016/J.MINENG.2011.10.010.
[23] A.R. Augustyn, R.W.M. Pott, M. Tadie, The interactions of the biosurfactant surfactin in coal flotation, Colloids Surf A Physicochem Eng Asp 627 (2021), 127122, https://doi.org/10.1016/J.COLSURFA.2021.127122.
[24] H. Khoshdast, A. Sam, H. Vali, K.A. Noghabi, Effect of rhamnolipid biosurfactants on performance of coal and mineral flotation, International Biodeterioration and Biodegradation 65 (2011) 1238–1243, https://doi.org/10.1016/J.IBIOD.2011.10.003.
[25] M. Kruszelnicki, I. Polowczyk, P.B. Kowalczuk, Control of glass surface wettability via esterification with n-alkyl alcohols, Physicochemical Problems of Mineral Processing. 58 (2022) 145147, https://doi.org/10.37190/PPMP/145147.
[26] F.K. Hansen, G. Rødsrud, Surface tension by pendant drop: I, A fast standard instrument using computer image analysis, J Colloid Interface Sci. 141 (1991) 1–9, https://doi.org/10.1016/0021-9797(91)90296-K.
[27] B. Song, J. Springer, Determination of Interfacial Tension from the Profile of a Pendant Drop Using Computer-Aided Image Processing: 2, Experimental, J Colloid Interface Sci. 184 (1996) 77–91, https://doi.org/10.1006/JCIS.1996.0598.
[28] J. Zawala, A. Niecikowska, "Bubble-on-demand" generator with precise adsorption time control, Rev. Sci. Instrum. 88 (2017), 095106, https://doi.org/10.1063/1.5001846.
[29] D. Kosior, J. Zawala, A. Niecikowska, K. Malysa, Influence of non-ionic and ionic surfactants on kinetics of the bubble attachment to hydrophilic and hydrophobic solids, Colloids Surf A Physicochem Eng Asp 470 (2015) 333–341, https://doi.org/10.1016/J.COLSURFA.2014.11.043.
[30] I.E. Kłosowska-Chomiczewska, K. Mędrzycka, E. Hallmann, E. Karpenko, T. Pokynbroda, A. Macierzanka, C. Jungnickel, Rhamnolipid CMC prediction, J. Colloid Interface Sci. 488 (2017) 10–19, https://doi.org/10.1016/J.JCIS.2016.10.055.
[31] A. Zdziennicka, B. Jańczuk, Thermodynamic parameters of some biosurfactants and surfactants adsorption at water-air interface, J. Mol. Liq. 243 (2017) 236–244, https://doi.org/10.1016/J.MOLLIQ.2017.08.042.
[32] H. Abbasi, K.A. Noghabi, M.M. Hamedi, H.S. Zahiri, A.A. Moosavi-Movahedi, M. Amanlou, J.A. Teruel, A. Ortiz, Physicochemical characterization of a monorhamnolipid secreted by Pseudomonas aeruginosa MA01 in aqueous media, An experimental and molecular dynamics study, Colloids Surf B Biointerfaces. 101 (2013) 256–265, https://doi.org/10.1016/J.COLSURFB.2012.06.035.
[33] G. Özdemir, S. Peker, S.S. Helvaci, Effect of pH on the surface and interfacial behavior of rhamnolipids R1 and R2, Colloids Surf A Physicochem Eng Asp 234 (2004) 135–143, https://doi.org/10.1016/J.COLSURFA.2003.10.024.
[34] J.M.R. Patino, M.R. Dominguez, J. de la FuenteFeria, The Effect of Sugars on Monostearin Monolayers, J. Colloid Interface Sci. 157 (1993) 343–354, https://doi.org/10.1006/JCIS.1993.1195.
[35] K.J. Legawiec, M. Kruszelnicki, A. Bastrzyk, I. Polowczyk, Rhamnolipids as Effective Green Agents in the Destabilisation of Dolomite Suspension, Int. J. Mol. Sci. 22 (2021) 10591, https://doi.org/10.3390/IJMS221910591.
[36] L. Martínez-Balbuena, A. Arteaga-Jiménez, E. Hernández-Zapata, C. Márquez-Beltrán, Applicability of the Gibbs Adsorption Isotherm to the analysis of experimental surface-tension data for ionic and nonionic surfactants, Adv. Colloid Interface Sci. 247 (2017) 178–184, https://doi.org/10.1016/J.CIS.2017.07.018.
[37] I. Mukherjee, S.P. Moulik, A.K. Rakshit, Tensiometric determination of Gibbs surface excess and micelle point: A critical revisit, J. Colloid Interface Sci. 394 (2013) 329–336, https://doi.org/10.1016/J.JCIS.2012.12.004.
[38] L. mei Wu, L. Lai, Q. Lu, P. Mei, Y. qun Wang, L. Cheng, Y. Liu,, Comparative studies on the surface/interface properties and aggregation behavior of mono-rhamnolipid and di-rhamnolipid, Colloids Surf. BBiointerfaces 181 (2019) 593–601, https://doi.org/10.1016/J.COLSURFB.2019.06.012.
[39] Y. bing Zhang, J. hua Chen, Y. qiong Li, P. xin Zhang,, Adsorption structures of frothers at gas-liquid interface using DFT method, J. Cent. South Univ. 26 (2019) 536–549, https://doi.org/10.1007/S11771-019-4025-7/METRICS.
[40] J.W. Drelich, A. Marmur, Meaningful contact angles in flotation systems: critical analysis and recommendations, Surf Innov. 6 (2018) 19–30, https://doi.org/10.1680/JSUIN.17.00037.

[41] A. Zdziennicka, B. Jańczuk, Wetting and adhesion properties of rhamnolipid and surfactin, Int. J. Adhes. Adhes. 84 (2018) 275–282, https://doi.org/10.1016/J.IJADHADH.2018.04.005.
[42] T. Young III, An essay on the cohesion of fluids, Philos. Trans. R. Soc. Lond. 95 (1805) 65–87, https://doi.org/10.1098/RSTL.1805.0005.
[43] K. Holmberg, B. Jönsson, B. Kronberg, B. Lindman, Adsorption of Surfactants at Solid Surfaces, in: Surfactants and Polymers in Aqueous Solution, John Wiley & Sons Ltd, 2004, pp. 357–387, https://doi.org/10.1002/0470856424.CH17.
[44] A. García-Prieto, L. Lunar, S. Rubio, D. Pérez-Bendito, Hemimicelle-based solid-phase extraction of estrogens from environmental water samples, Analyst 131 (2006) 407–414, https://doi.org/10.1039/B514100A.
[45] R. Atkin, V.S.J. Craig, S. Biggs, Adsorption kinetics and structural arrangements of cationic surfactants on silica surfaces, Langmuir 16 (2000) 9374–9380, https://doi.org/10.1021/LA0001272/ASSET/IMAGES/LARGE/LA0001272F00009.JPEG.
[46] R. Zhang, P. Somasundaran, Advances in adsorption of surfactants and their mixtures at solid/solution interfaces, Adv. Colloid Interface Sci. 123–126 (2006) 213–229, https://doi.org/10.1016/J.CIS.2006.07.004.
[47] M. Kruszelnicki, I. Polowczyk, P.B. Kowalczuk, Control of glass surface wettability via esterification with n-alkyl alcohols, Physicochemical Problems of Mineral Processing. 58 (2021) 145147, https://doi.org/10.37190/PPMP/145147.
[48] J. Zawala, Energy balance in viscous liquid containing a bubble: Rise due to buoyancy, Can. J. Chem. Eng. 94 (2016) 586–595, https://doi.org/10.1002/CJCE.22420.
[49] R. Manica, E. Klaseboer, D.Y.C. Chan, The impact and bounce of air bubbles at a flat fluid interface, Soft Matter 12 (2016) 3271–3282, https://doi.org/10.1039/C5SM03151F.
[50] M. Wegener, N. Paul, M. Kraume, Fluid dynamics and mass transfer at single droplets in liquid/liquid systems, Int. J. Heat Mass Transf. 71 (2014) 475–495, https://doi.org/10.1016/J.IJHEATMASSTRANSFER.2013.12.024.
[51] S.S. Dukhin, R. Miller, G. Loglio, Physico-chemical hydrodynamics of rising bubble, Studies in Interface Science. 6 (1998) 367–432, https://doi.org/10.1016/S1383-7303(98)80025-2.
[52] J. Zawala, D. Kosior, K. Malysa, Formation and influence of the dynamic adsorption layer on kinetics of the rising bubble collisions with solution/gas and solution/solid interfaces, Adv. Colloid Interface Sci. 222 (2015) 765–778, https://doi.org/10.1016/J.CIS.2014.07.013.
[53] J. Zawala, J. Miguet, P. Rastogi, O. Atasi, M. Borkowski, B. Scheid, G.G. Fuller, Coalescence of surface bubbles: The crucial role of motion-induced dynamic adsorption layer, Adv. Colloid Interface Sci. 317 (2023), 102916, https://doi.org/10.1016/J.CIS.2023.102916.
[54] K.J. Stebe, S.Y. Lin, C. Maldarelli, Remobilizing surfactant retarded fluid particle interfaces. I. Stress-free conditions at the interfaces of micellar solutions of surfactants with fast sorption kinetics, Physics of Fluids A, Fluid Dyn. 3 (1998) 3, https://doi.org/10.1063/1.857862.
[55] K.W. Stöckelhuber, Stability and rupture of aqueous wetting films, The, European Physical Journal E 12 (2004) 431–435, https://doi.org/10.1140/EPJE/E2004-00012-9.
[56] K.W. Stöckelhuber, B. Radoev, A. Wenger, H.J. Schulze, Rupture of Wetting Films Caused by Nanobubbles, Langmuir 20 (2004) 164–168, https://doi.org/10.1021/LA0354887/ASSET/IMAGES/LARGE/LA0354887F00005.JPEG.
[57] A. Niecikowska, M. Krasowska, J. Ralston, K. Malysa, Role of surface charge and hydrophobicity in the three-phase contact formation and wetting film stability under dynamic conditions, J. Phys. Chem. C 116 (2012) 3071–3078, https://doi.org/10.1021/JP211378S/SUPPL_FILE/JP211378S_SI_001.PDF.
[58] J. Zawala, C. Karaguzel, A. Wiertel, O. Sahbaz, K. Malysa, Kinetics of the bubble attachment and quartz flotation in mixed solutions of cationic and non-ionic surface-active substances, Colloids Surf A Physicochem Eng Asp 523 (2017) 118–126, https://doi.org/10.1016/J.COLSURFA.2017.03.063.
[59] M. Kosmulski, The pH dependent surface charging and points of zero charge. VII. Update, Adv. Colloid Interface Sci. 251 (2018) 115–138, https://doi.org/10.1016/J.CIS.2017.10.005.
[60] C. Yang, T. Dabros, D. Li, J. Czarnecki, J.H. Masliyah, Measurement of the Zeta Potential of Gas Bubbles in Aqueous Solutions by Microelectrophoresis Method, J. Colloid Interface Sci. 243 (2001) 128–135, https://doi.org/10.1006/JCIS.2001.7842.
[61] J. Zawala, K. Malysa, Influence of the impact velocity and size of the film formed on bubble coalescence time at water surface, Langmuir 27 (2011) 2250–2257, https://doi.org/10.1021/LA104324U/ASSET/IMAGES/LARGE/LA-2010-04324U_0010.JPEG.
[62] R. Cohen, G. Ozdemir, D. Exerowa, Free thin liquid films (foam films) from rhamnolipids: type of the film and stability, Colloids Surf. BBiointerfaces 29 (2003) 197–204, https://doi.org/10.1016/S0927-7765(02)00209-6.
[63] R. Cohen, D. Exerowa, Surface forces and properties of foam films from rhamnolipid biosurfactants, Adv. Colloid Interface Sci. 134–135 (2007) 24–34, https://doi.org/10.1016/J.CIS.2007.04.018.
[64] H. Khoshdast, H. Abbasi, A. Sam, K.A. Noghabi, Frothability and surface behavior of a rhamnolipid biosurfactant produced by Pseudomonas aeruginosa MA01, Biochem. Eng. J. 60 (2012) 127–134, https://doi.org/10.1016/J.BEJ.2011.10.015.
[65] J. Radulovic, K. Sefiane, V.M. Starov, N.S. Ivanova, Review on Kinetics of Spreading and Wetting by Aqueous Surfactant Solutions, in: M. Ferrari, L. Liggeri, R. Miller (Eds.), Drops and Bubbles in Contact With Solid Surfaces, CRC Press, Boca Raton, 2013.
[66] P. Basarova, T. Vachova, G. Moore, G. Nannetti, J. Pislova, Bubble adhesion onto the hydrophobic surface in solutions of non-ionic surface-active agents, Colloids Surf A Physicochem Eng Asp 505 (2016) 64–71, https://doi.org/10.1016/J.COLSURFA.2015.11.069.
[67] P. Basarova, H. Suchanova, K. Souskova, T. Vachova, Bubble adhesion on hydrophobic surfaces in solutions of pure and technical grade ionic surfactants, Colloids Surf A Physicochem Eng Asp 522 (2017) 485–493, https://doi.org/10.1016/J.COLSURFA.2017.03.024.